APL Materials

Topological insulators for efficient spin–orbit torques

Cite as: APL Mater. **9**, 060901 (2021); https://doi.org/10.1063/5.0048619
Submitted: 24 February 2021 • Accepted: 13 May 2021 • Published Online: 25 May 2021

Jiahao Han and Luqiao Liu

COLLECTIONS

Paper published as part of the special topic on Emerging Materials for Spin-Charge Interconversion

openaccess

View Online Export Citation CrossMark

ARTICLES YOU MAY BE INTERESTED IN

Spin-orbit torques: Materials, physics, and devices
Applied Physics Letters **118**, 120502 (2021); https://doi.org/10.1063/5.0039147

Spin–orbit torque characterization in a nutshell
APL Materials **9**, 030902 (2021); https://doi.org/10.1063/5.0041123

Field-free magnetization switching induced by the unconventional spin–orbit torque from WTe_2
APL Materials **9**, 051114 (2021); https://doi.org/10.1063/5.0048926

© 2021 Author(s).

AIP Publishing

Topological insulators for efficient spin–orbit torques

Cite as: APL Mater. 9, 060901 (2021); doi: 10.1063/5.0048619
Submitted: 24 February 2021 • Accepted: 13 May 2021 •
Published Online: 25 May 2021

View Online Export Citation CrossMark

Jiahao Han and Luqiao Liu[a)]

AFFILIATIONS

Department of Electrical Engineering and Computer Science, Massachusetts Institute of Technology, Cambridge, Massachusetts 02139, USA

Note: This paper is part of the Special Topic on Emerging Materials for Spin-Charge Interconversion.
[a)]**Author to whom correspondence should be addressed:** luqiao@mit.edu

ABSTRACT

Current-induced magnetic switching via spin–orbit torques has been extensively pursued for memory and logic applications with promising energy efficiency. Topological insulators are a group of materials with spin-momentum locked electronic states at the surface due to spin–orbit coupling, which can be harnessed to reach strong spin–orbit torques. In this paper, we summarize and compare the methods for calibrating the charge-spin conversion efficiency in topological insulators, with which topological insulators are identified as outstanding spin–orbit torque generators compared with the well-studied heavy metals. We then review the results of magnetic switching under reduced current density in topological insulator/ferromagnet heterostructures. Finally, we provide insights on current challenges as well as possible exploration directions in the emerging field of topological spintronics.

© 2021 Author(s). All article content, except where otherwise noted, is licensed under a Creative Commons Attribution (CC BY) license (http://creativecommons.org/licenses/by/4.0/). https://doi.org/10.1063/5.0048619

I. INTRODUCTION

In the past decade of spintronic studies, current-induced magnetic switching via spin–orbit torques (SOTs) has been extensively pursued as a promising technique for writing information in the magnetic random-access memory with low power consumption, unlimited endurance, and fast operation time.[1] The key to generate strong SOTs is to find materials with large spin–orbit coupling that can convert charge current into non-equilibrium spins to interact with magnetic moments. Heavy metals such as Pt,[2,3] Ta,[4] and W[5] were among the first that have been utilized to generate non-equilibrium spins via the spin Hall effect or the Rashba–Edelstein effect. The spin Hall effect[6] converts a three-dimensional charge current density $\boldsymbol{J}_c$ (in the unit of A/m^2) to a transverse spin current density $(2e/\hbar)\boldsymbol{J}_s$ (in the unit of A/m^2; e is the electron charge and $\hbar$ is the reduced Planck's constant) with spin polarization $\boldsymbol{\sigma}$. The spin current is expressed as $(2e/\hbar)\boldsymbol{J}_s = \theta_{SH}\boldsymbol{\sigma} \times \boldsymbol{J}_c$, with θ_{SH} being the unitless spin Hall angle. Besides the spin Hall effect in the bulk, the Rashba–Edelstein effect of the two-dimensional electron states at the surface can be another mechanism to generate spin polarization.[7] The injected two-dimensional charge current density ($\boldsymbol{j}_c$, in the unit of A/m) can be converted to a three-dimensional spin current density $(2e/\hbar)\boldsymbol{J}_s$ via the Rashba–Edelstein-effect coefficient (q, in the unit of nm^{-1}) expressed as[8] $(2e/\hbar)\boldsymbol{J}_s = q\boldsymbol{\sigma} \times \boldsymbol{j}_c$. When neighbored by a ferromagnetic material with magnetic moment $\boldsymbol{m}$, the non-equilibrium spins $\boldsymbol{\sigma}$ can exert SOTs to modulate the magnetic dynamics or even switch the magnetic orientation, which enables the core function of magnetic memory and logic devices. In general, the SOTs can be decomposed to a field-like term $\boldsymbol{\tau}_{FL} \sim \boldsymbol{\sigma} \times \boldsymbol{m}$ and a damping-like term $\boldsymbol{\tau}_{DL} \sim \boldsymbol{m} \times (\boldsymbol{\sigma} \times \boldsymbol{m})$, the latter of which usually accounts for magnetic switching.[1] It is worth noting that the generation of damping-like torques is not restricted to the categories of conventional spin-transfer torques or spin Hall effect-induced SOTs. The non-equilibrium spin $\boldsymbol{\sigma}$ from both bulk and interfacial spin–orbit coupling can give rise to $\boldsymbol{\tau}_{DL}$ when $\boldsymbol{\sigma}$ is absorbed by the adjacent magnetic material via spin flipping scattering.[1,9,10]

The recent discovery of topological insulators (TIs) provides tremendous opportunities to further improve the efficiency of charge-spin conversions. TIs are a class of materials with spin–orbit coupling that is strong enough to invert the sequence of bands at certain high symmetry points and leads to topologically protected

© Author(s) 2021

conducing electronic states at the surfaces[11–14] [Fig. 1(a)]. The topological surface states exhibit a helical Dirac cone character in the dispersion relation, where the spin orientation of electrons is locked with their wavevector [Figs. 1(b) and 1(c)]. When a charge current flows through the surface, which can be described in the wavevector space as a shift in the electron distribution at the Fermi surface, the number of forward-going electrons dominates over backward-going ones, leading to a net spin accumulation because of the spin-momentum locking[15,16] [Fig. 1(d)].

Compared to heavy metals, TIs can, in principle, provide much higher non-equilibrium spin accumulation with the same amount of charge current. The bulk band topology in TIs gives rise to topological surface states with one-to-one locking for spin and momentum orientations.[8] With an applied charge current, this mechanism provides higher spin accumulation than the Rashba spin–orbit coupling that causes two surface bands with opposite spin-momentum locking chirality. Here, we note that because of the bulk–surface correspondence, the surface states of TI can also be viewed as a holographic manifestation of the bulk topology.[17] We treat the contributions from the intrinsic topologically determined bulk band as the same with the one from the topological surface state. Besides the surface spin-momentum locking, exotic spin–orbit effects in TIs may lead to large spin accumulation from the bulk states[18–20] through extrinsic non-topological mechanisms as well.

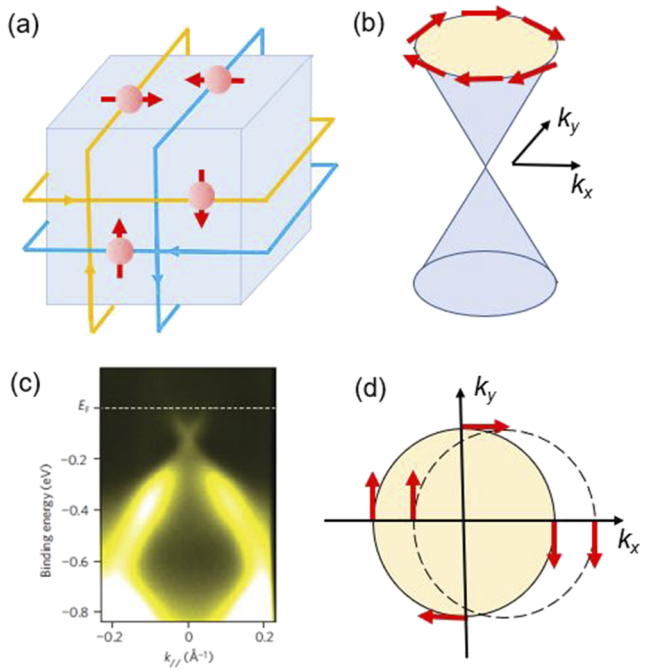

FIG. 1. Topological surface states and spin-momentum locking in TIs. (a) Real space picture of the conducting surface states in an ideal TI. (b) Dirac cone of the topological surface states in the wavevector space, where the spin and momentum of electrons are one-to-one locked to each other at the Fermi level. (c) Angle-resolved photoemission spectrum that indicates the bulk and surface bands of a six-quintuple-layer-thick Bi_2Se_3 film. (d) Top view of the Dirac cone crossed by the Fermi level with spin-momentum locking. With a flow of charge current, the shift in the electron distribution in the wavevector space induces non-equilibrium spins. Panel (c) is adapted with permission from Zhang *et al.*, Nat. Phys. **6**, 584 (2010). Copyright 2010 Springer Nature Limited.

Thanks to the development of advanced material growth and characterization techniques in the past decades, various TI thin films have been synthesized and have been demonstrated to own non-trivial topological electronic structures via the angle-resolved photoemission spectroscopy (ARPES).[21–23] These efforts provide the foundation for exploiting TI thin films in spintronic devices as efficient SOT sources. So far, the most extensively studied group of TIs is the bismuth-based compounds including Bi_xSb_{1-x}, Bi_2Se_3, Bi_2Te_3, $(Bi_xSb_{1-x})_2Te_3$, and so on,[13,14,21,24] grown by molecular beam epitaxy, which allows one to precisely control the layer-by-layer growth of the epitaxial structure. Whereas the Fermi surface in Bi_xSb_{1-x}, Bi_2Se_3, and Bi_2Te_3 usually intersects with the bulk bands, the tunable Bi:Sb ratio in $(Bi_xSb_{1-x})_2Te_3$ allows one to adjust the Fermi level to within the bandgap of the bulk states[21,24] so that only the topological surface states are conductive. Other TI materials such as α-Sn[25] and SmB_6[26–29] have also demonstrated topological bands that enable charge-spin conversion. Very recently, magnetron sputtering, a technique that has been widely adapted in semiconductor manufacturing, has been utilized to grow TI compounds with giant charge-spin conversion.[30]

In Secs. II and III, we will review the major progresses toward the goal of utilizing TIs for efficient magnetic switching, which involves determinations of SOT efficiency generated by TIs, experimental demonstrations of magnetic switching with TI heterostructures, and optimization of the magnetic switching at room temperature to make TIs compatible with practical application considerations.

II. QUANTIFICATION OF THE SPIN–ORBIT TORQUE EFFICIENCY

Two pioneering works that explore the SOT generated by TIs were reported in 2014 by Fan *et al.*[31] and Mellnik *et al.*[32] independently. Fan *et al.* utilized the second harmonic magnetometry, which was first applied to bilayers of heavy metal/ferromagnetic films with perpendicular magnetic anisotropy (PMA),[33,34] to calibrate the SOT effective field in the Cr-$(Bi_xSb_{1-x})_2Te_3$/$(Bi_xSb_{1-x})_2Te_3$ (magnetically doped TI/intrinsic TI) heterostructure at a temperature of 1.9 K.[31] In this method, a low-frequency alternating current is injected to generate the SOT and induces low-frequency oscillations of magnetic moments. The periodic change in the anomalous Hall resistance further accounts for the generation of the second harmonic component of the Hall voltage [Fig. 2(a)]. The voltage detection can also be replaced by the magneto-optic Kerr signal that is sensitive to magnetic moment tiltings,[35] where the effective spin Hall angle is determined to be 90 at a temperature of 2.5 K and decreases dramatically as the temperature increases.

In the room-temperature experiment done by Mellnik *et al.*, an electrical current with microwave frequency is injected into the Bi_2Se_3/NiFe bilayer.[32] The SOT generated by the oscillating current in Bi_2Se_3 causes resonant precession of the NiFe magnetization, yielding resistance oscillations due to the anisotropic magnetoresistance effect.[36] The mixing between the applied alternating current and the oscillating resistance leads to a direct voltage, from which the magnitude of the damping-like (in-plane) and field-like

© Author(s) 2021

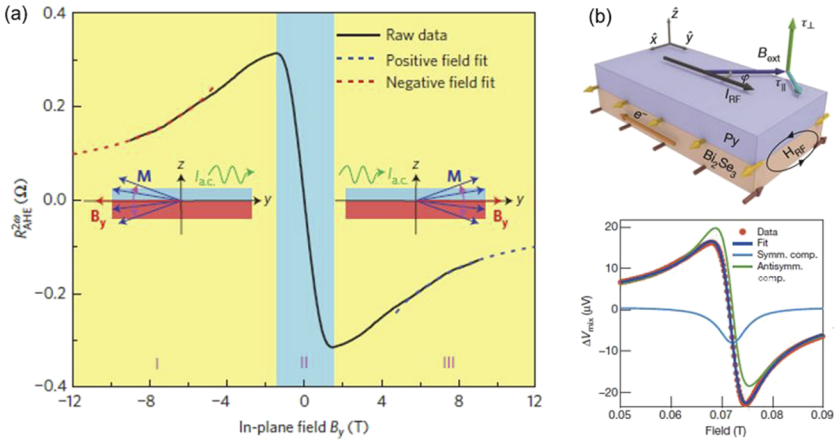

FIG. 2. Experimental proof of the SOT generated from TIs. (a) Second-harmonic anomalous Hall resistance as a function of in-plane external magnetic field, measured in the Cr-$(Bi_xSb_{1-x})_2Te_3$/$(Bi_xSb_{1-x})_2Te_3$ sample. The shaded regions I, II, and III represent a single-domain state pointing in the $-y$ direction, magnetization reversal, and a single-domain state pointing in the $+y$ direction, respectively. The insets in regions I and III show the tilted magnetization around its equilibrium position under a low-frequency alternating current. (b) Top panel: schematic of the spin-torque ferromagnetic resonance setup for a Bi_2Se_3/NiFe sample. The radio frequency current I_{RF} genereates net spin accumulation and thus the spin torques τ on the NiFe moments. Bottom panel: mixing voltage measured in the spin-torque ferromagnetic resonance experiment. Panel (a) is adapted with permission from Fan *et al.*, Nat. Mater. **13**, 699 (2014). Copyright 2014 Springer Nature Limited. Panel (b) is adapted with permission from Mellnik *et al.*, Nature **511**, 449 (2014). Copyright 2014 Springer Nature Limited.

(out-of-plane) SOT can be extracted [Fig. 2(b)]. The determined effective spin Hall angle, which represents the damping-like SOT strength per unit current density, is an order of magnitude higher than the heavy metals, pointing toward the strategy of realizing low-power magnetic memory devices using TIs as room-temperature SOT sources. A temperature-dependent study further reveals that the topological surface states are mostly responsible for the SOT in this TI at low temperature.[37] Here, we note that although the spin Hall angle was originally defined for the spin Hall effect, it is often used as a general figure of merit to reflect the SOT efficiency even when the exact mechanism is not the conventional three-dimensional spin Hall effect. This effective term of the spin Hall angle is defined as the ratio between the spin current density, calculated from the detected SOT, and the averaged charge current density across the thickness of the spin–orbit material.

The third method usually used for quantifying SOT is the domain wall magnetometry approach, where a direct current and a constant biasing magnetic field are applied simultaneously. Within chiral domain walls, the SOT acts as an effective field in the out-of-plane direction for the magnetic thin film with PMA. The SOT effective field can assist or impede the domain wall movement and thus the magnetic switching, which is reflected by a shift in the coercive field in anomalous Hall resistance measurement when sweeping an out-of-plane field[38] [Figs. 3(a) and 3(b)]. In this method, the SOT is directly compared with applied magnetic fields rather than changes in Hall resistance, which prevents the parasitic contributions from complicated transport phenomena in TIs.[39,40] As expected, the SOT efficiency still exceeds that of heavy metals detected by the same protocol.[41]

Being the reciprocal effect of the SOT-induced ferromagnetic resonance, spin pumping is a representative method to verify the spin-to-charge conversion in TIs. By exciting magnetic resonance via the inductive method in a ferromagnet, spin current is injected to the neighbored TI layer, which is converted to a charge current through the surface spin-momentum locking or the bulk inverse spin Hall effect[19,20,42,43] [Figs. 3(c) and 3(d)]. Among the experiments in bismuth-based TIs, although the reported spin pumping phenomena are qualitatively consistent, the spin-to-charge conversion ratio, characterized by the effective spin Hall angle (ratio between the averaged charge current density and the spin current density), varies by several orders of magnitude (10^{-4} to 10^{1}). The origin of the large discrepancy is still inconclusive but possibly comes from the following aspects: (i) differences in measurement temperature and element doping, which modulates the proportion of surface and bulk conductivities; (ii) parasitic effects with the spin pumping when TI is accompanied with a metallic ferromagnet, in particular, the spin rectification effect originating from microwave irradiation or thermal effects;[44–46] and (iii) variation of film thickness and interface quality during the sample preparation. In addition to giving rise to a spin pumping voltage, it has been shown that the spin-charge interconversion and the exchange interaction from the topological surface states can lead to phenomena such as enhanced Gilbert damping and additional magnetic anisotropy on magnetic materials, which modulates their ferromagnetic resonance behaviors.[47–50] Besides the experiments discussed above that utilize SOTs to modulate magnetic orientation or oscillation, other magneto-transport methods such as spin Seebeck effect,[51] lateral spin valve,[52–59] tunneling spectroscopy,[60] and bilinear magnetoelectric resistance[61] have been utilized to confirm the robust charge-spin interconversion in TIs as well.

The surface spin-momentum locking mechanism can be studied from the dependence of the spin-charge conversion on the Fermi level position. For the purpose of emphasizing the two-dimensional nature of the surface states, the ratio between the two-dimensional

© Author(s) 2021

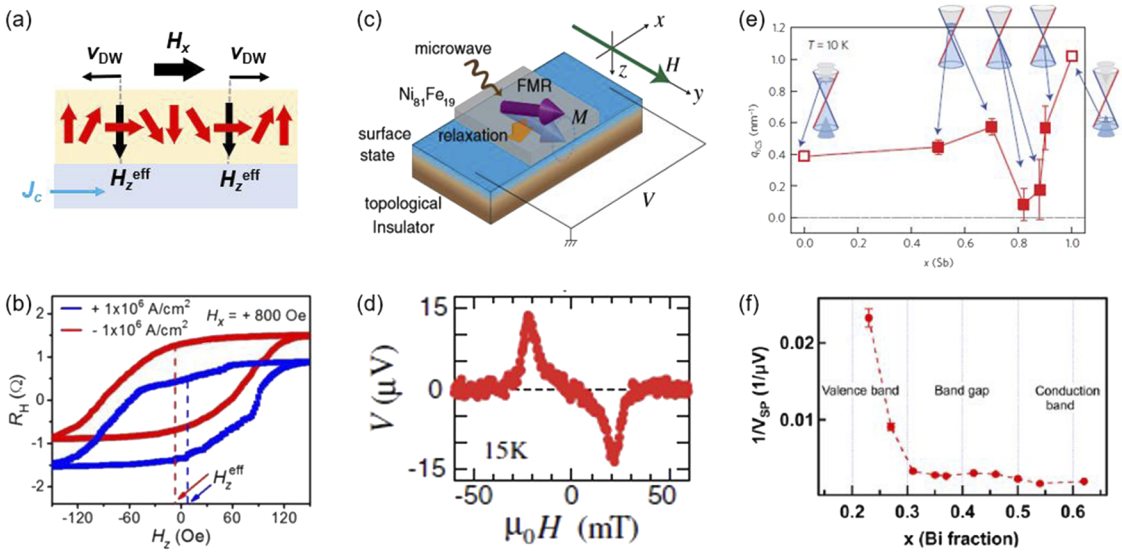

FIG. 3. Magnetotransport and dynamic measurements of the charge-spin conversions in TIs. (a) SOT-driven domain wall motion in a PMA layer under an in-plane magnetic field H_x, which fixes the domain wall chirality. The domain wall moments experience an effective SOT field H_z^{eff} along the out-of-plane direction and move along the opposite directions, as indicated by the domain wall velocity v_{DW}. (b) Hall resistance vs applied out-of-plane field under positive and negative direct currents and an in-plane bias field in the Bi_2Se_3/CoTb sample. The center shift corresponds to the SOT effective field (H_z^{eff}). (c) Schematic of the spin pumping from NiFe to a TI layer. (d) Spin pumping voltage in the $Bi_{1.5}Sb_{0.5}Te_{1.7}Se_{1.3}$/NiFe sample. (e) Interface charge-to-spin conversion efficiency q_{ICS} as a function of Sb composition x in $(Bi_xSb_{1-x})_2Te_3$, measured by spin-torque ferromagnetic resonance. The inset shows the band structure and Fermi level position for samples with different Sb concentrations. $(Bi_xSb_{1-x})_2Te_3$ with conductive surface states and insulating bulk states are expected to exist with $0.5 < x < 0.9$. (f) Spin pumping voltage as a function of Bi ratio x in $Cr_{0.08}(Bi_xSb_{1-x})_{1.92}Te_3/Y_3Fe_5O_{12}$. Panel (b) is adapted with permission from Han *et al.*, Phys. Rev. Lett. **119**, 077702 (2017). Copyright 2017 American Physical Society. Panels (c) and (d) are adapted with permission from Shiomi *et al.*, Phys. Rev. Lett. **113**, 196601 (2014). Copyright 2014 American Physical Society. Panel (e) is adapted with permission from Kondou *et al.*, Nat. Phys. **12**, 1027 (2016). Copyright 2016 Springer Nature Limited. Panel (f) is adapted with permission from Wang *et al.*, Phys. Rev. Res. **1**, 012014(R) (2019). Copyright 2019 American Physical Society.

charge current density j_c and the three-dimensional spin current density J_s in the Rashba–Edelstein configuration is more appropriate to describe the conversion efficiency. Via the spin-torque ferromagnetic resonance in $(Bi_xSb_{1-x})_2Te_3$, Kondou *et al.* found that for x = 0.5, 0.7, and 0.9, where the Fermi level falls into the bulk bandgap but is apart from the Dirac point, the charge-to-spin conversion ratio $q = (2eJ_s)/(\hbar j_c)$ (in the unit of nm^{-1}) is almost constant.[62] This is because in this range, only the topological surface states are conductive and contribute to the charge-to-spin conversion [Fig. 3(e)]. An additional feature in this experiment is the small value of q when the Fermi level is very close to the Dirac point. As pointed out in Ref. 62, this effect may come from (i) the inhomogeneities in the surface states around the Dirac point, which deviates the charge flow from the electric field direction and weaken the net spin accumulation, and (ii) the spacer layer may induce an additional Rashba spin splitting and partially cancel the spin-momentum locking effect. On the other hand, using second harmonic measurement and current-induced switching, Wu *et al.*[63] showed that the SOT effective field reaches maximum when the Fermi level lies in the bulk bandgap. This is consistent with another Fermi level dependent SOT measurement, where the Fermi level position is tuned by a gate voltage.[64] It is shown that when the Fermi level only intersects with the surface band, the SOT efficiency is larger than the bulk conducting case. The application of gate voltage provides an additional degree of freedom to control SOT. Moreover, in a spin pumping experiment with $Cr_{0.08}(Bi_xSb_{1-x})_{1.92}Te_3/Y_3Fe_5O_{12}$ bilayers, Wang *et al.*[17] observed a constant spin pumping signal when the Fermi level is tuned within the bulk bandgap [Fig. 3(f)]. This is consistent with the unchanged charge-to-spin conversion efficiency in the direct measurements on SOT when the conductivity only comes from the surface states. We note that the usage of the ferromagnetic insulator as the spin current source[17,65] excludes possible artifacts brought by conductive ferromagnets.

The charge-spin conversion efficiency is also influenced by the TI thickness t, which can reflect the conversion mechanism of the interfacial spin-momentum locking or the bulk spin Hall effect. First, for an ideal TI, the spin-to-charge conversion is expected to be solely originated from surface states (with thickness t_s). It is also assumed that only the surface conducts current and the bulk is insulating. Under a fixed spin injection current density (J_s), the spin pumping charge current I_{sp} will first increase and then saturate with t. The saturation point corresponds to a complete separation of the top and bottom surfaces ($t > 2t_s$) [Fig. 4(a)]. Because increasing the bulk thickness does not contribute to the conductivity of an ideal TI, the spin pumping voltage V_{sp} is expected to have a platform as well for $t > 2t_s$ [Fig. 4(b)]. Meanwhile, for the three-dimensional spin Hall effect, I_{sp} increases and gradually saturates with t after exceeding $2\lambda_{sf}$, where λ_{sf} denotes the spin diffusion length [Fig. 4(c)]. As t increases, V_{sp} should have a decreasing behavior, which is from the reduced resistance [Fig. 4(d)].

© Author(s) 2021

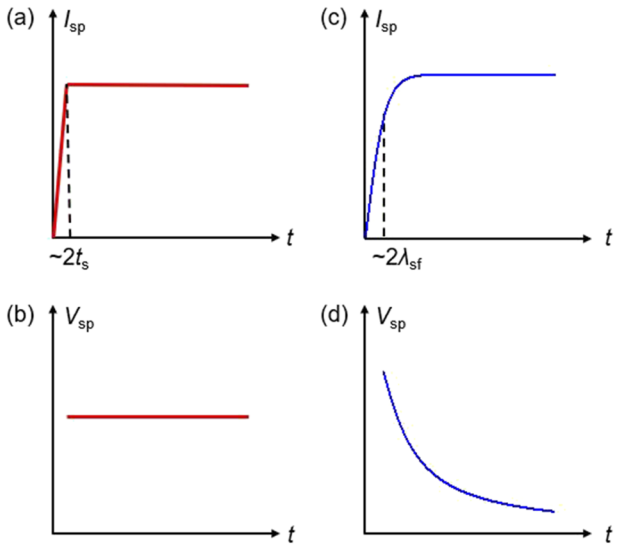

FIG. 4. Thickness t dependence of the spin pumping signals. [(a) and (b)] Spin pumping charge current I_{sp} and voltage V_{sp} in an ideal TI, where the surface states with a thickness of t_s solely provide the conductivity and the spin-to-charge conversion through spin-momentum locking. [(c) and (d)] I_{sp} and V_{sp} in a system with a conducting bulk and the (inverse) spin Hall effect. λ_{sf} represents the spin diffusion length.

Now, by comparing Fig. 4(a) with Fig. 4(c), and Fig. 4(b) with Fig. 4(d), one can see that the biggest difference between the ideal TI and spin Hall effect is that V_{sp} remains constant in the large thickness limit for the TI case due to the insulating bulk state. However, in real TIs studied so far (with thickness dependence), the bulk state is often not fully insulating. Therefore, V_{sp} also decreases with t, as reported in Ref. 65, because Bi_2Se_3 is bulk conducting. On the other hand, I_{sp} saturates at a small thickness of ~2 nm in Ref. 65, but at a much larger thickness of ~30 nm in Ref. 19. These values may be correlated with the surface thickness in TI and a possibly larger spin diffusion length in a metal-like system, respectively. Furthermore, in polycrystalline films, the thickness dependence can be influenced by size effects, such as the charge-spin conversion from quantum confinement in granular Bi_xSe_{1-x} films (see more details in Sec. III).

III. SPIN–ORBIT TORQUE SWITCHING INDUCED BY TOPOLOGICAL INSULATORS

Current-induced magnetic switching via the giant SOT from TIs was realized for the first time in the Cr-$(Bi_xSb_{1-x})_2Te_3$/$(Bi_xSb_{1-x})_2Te_3$ heterostructures[31] and later in Cr-$(Bi_xSb_{1-x})_2Te_3$ sandwiched by different insulators,[64] where the Cr-doped TI becomes magnetic with PMA at cryogenic temperatures [Fig. 5(a)]. The magnetic reversal is reflected by the sign change of the anomalous Hall resistance when sweeping the direct current, which has been extensively used in the SOT switching experiments in heavy/metal/ferromagnet structures. At an experimental temperature of 1.9 K, the critical switching current below 10^5 A/cm^2 (two orders of magnitude smaller than the typical values of heavy metals) stimulated significant interest in pursuing ultralow power dissipation memory and logic devices using TIs. In later studies, to suppress possible extra electrical contributions from TI heterostructures,[39] Yasuda *et al.*[39] and Che *et al.*[35] developed another method of using pulsed current to induce magnetic switching and direct current with a much weaker amplitude to sense the Hall resistance. The critical current density with a slightly larger magnitude is still far below that of heavy metals.

Due to the low Curie temperature of the employed ferromagnetic materials, magnetic switching was only realized at a few Kelvin in the magnetically doped TI heterostructures. Room temperature SOT switching, which is critical for most applications, requires the development of ferromagnetic thin films with appropriate anisotropy (PMA or uniaxial in-plane anisotropy) when accompanied with TI. So far, progresses have been made using different strategies. The first is to utilize rare earth-transition metal alloys, in which two magnetic sublattices are antiferromagnetically coupled. The PMA is realized through the growth-induced strain in the bulk and is less sensitive to the underlayer structures.[66,67] In the CoTb/Bi_2Se_3 bilayer, Han *et al.* demonstrated room-temperature SOT switching[41] [Fig. 5(b)], with the SOT efficiency several times higher than heavy metals Pt and Ta. This approach was also verified in other similar structures[68] such as Bi_2Se_3/GdFeCo and $(Bi_xSb_{1-x})_2Te_3$/GdFeCo. We note that the SOT efficiencies obtained

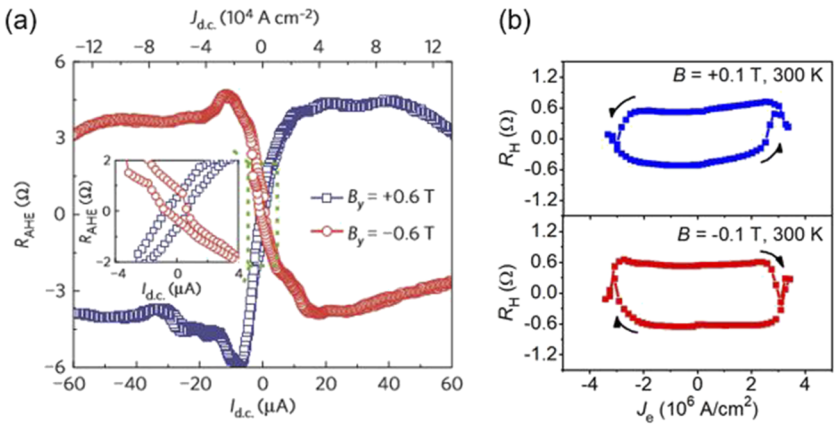

FIG. 5. Current-induced magnetic switching in TI based heterostructures with PMA. (a) Switching in the Cr-$(Bi_xSb_{1-x})_2Te_3$/$(Bi_xSb_{1-x})_2Te_3$ sample at 1.9 K. (b) Switching in the Bi_2Se_3/CoTb sample at room temperature. Panel (a) is adapted with permission from Fan *et al.*, Nat. Mater. **13**, 699 (2014). Copyright 2014 Springer Nature Limited. Panel (b) is adapted with permission from Han *et al.*, Phys. Rev. Lett. **119**, 077702 (2017). Copyright 2017 American Physical Society.

© Author(s) 2021

from the rare earth-transition metal alloys are usually smaller than those obtained from the traditional ferromagnetic electrodes, which is potentially due to a lower interfacial spin transparency in these stacks. In these experiments, it is shown that $(Bi_xSb_{1-x})_2Te_3$ with a more insulating bulk provides higher efficiency for magnetic switching than Bi_2Se_3, suggesting that the SOT generation benefits from a more concentrated charge current in topological surface states.[41,68] The second way is to grow an ultrathin non-magnetic seeding layer above TI, which gives rise to the needed texture for reaching PMA in the ferromagnetic layer grown on top. PMA multilayers such as Ti (or Mo)/CoFeB/MgO and Ta/CoFeB/Gd/CoFeB have been grown on TIs for magnetic switching.[30,63,69] In these multilayers, because of the small value or the opposite sign of the spin Hall angle, contributions from the non-magnetic seeding metals can be excluded and the dominant source of the SOT is identified to be the TI layer. In these stacks, the SOT efficiency is usually enhanced when the bulk of the TI is tuned to be less conductive, suggesting the important role of the topological surface states. The third method is to develop ferromagnetic films that are epitaxial on top of TIs, which provides correct crystal orientation and stain to generate PMA. For example, the epitaxial structure of $Bi_{0.9}Sb_{0.1}$/MaGa[70] shows a giant effective spin Hall angle of 52 and a low switching current density of 10^5 A/cm^2. The fourth method is to develop in-plane magnets whose easy-axis is collinear with the injected spin so that the magnetic moment can be switched by the SOT that overcomes the Gilbert damping. This configuration has been verified in the Bi_2Se_3/NiFe bilayer by the magneto-optic Kerr imaging.[71] It is also possible to electrically probe the in-plane magnetic reversal via the unidirectional magnetoresistance effects.[72–74]

In parallel with the strategy that utilizes topological surface states in epitaxial TI films, exploring novel TI compounds with exotic grain effects provide another approach for generating giant SOT. Using the SOT from the Bi_xSe_{1-x} thin films prepared by magnetron sputtering, Dc *et al.* observed switching of the CoFeB-based PMA multilayers at room temperature,[30] with a critical switching current density in the order of 10^5 A/cm^2. In the polycrystalline Bi_xSe_{1-x} film, the band structure of grains with reduced dimensions reveals additional states that have surface character and are localized mainly on the grain sidewalls and corner. Such a quantum confinement effect leads to a charge-to-spin conversion efficiency that enhances with reduced size and dimensionality of the nanoscale grains. The high spin-to-charge conversion was verified by the spin pumping experiment later,[75] in which the spin pumping signal decreases in thicker granular Bi_xSe_{1-x} films. This trend suggests that the enhanced quantum confinement in thinner films is critical to the large charge-spin conversion. Besides Bi_xSe_{1-x}, high SOT efficiency was also obtained in sputtered Bi_2Te_3 films.[76] These works highlight the potential of fabricating TI-based spintronic devices on silicon substrates using industry friendly techniques.

In TI/metallic ferromagnet stacks, the high resistivity of TIs usually causes significant current shunting through the ferromagnetic layer. One strategy to fully exploit the efficiency of TI is to utilize magnetic insulators as the free layer for switching. Potential candidates include rare earth iron garnets or barium ferrites with PMA.[77,78] Li *et al.*[78] reported switching of an insulating ferromagnet $BaFe_{12}O_{19}$ using the SOT from Bi_2Se_3. The switching efficiency at 3 K was found to be 300 times higher than that at room temperature and 30 times higher than that in Pt/$BaFe_{12}O_{19}$. The decreasing trend of the SOT efficiency with temperature is consistent with a number of reports in TI-based systems and suggests the presence of more pronounced topological surface states at low temperatures. Another approach to avoid shunting is to separate the TI and the conductive ferromagnet by inserting an insulating magnetic layer that blocks charge current, which, on the other hand, allows the transmission of spin angular momentum in the form of spin wave or spin fluctuations. In the Bi_2Se_3/NiO/NiFe trilayer structure, Wang *et al.*[79] demonstrated that the non-equilibrium spins generated from Bi_2Se_3 can transmit through the antiferromagnetic insulator NiO up to 25 nm and switch the NiFe moments.

Finally, we summarize from the literature the key features and parameters in the SOT switching experiments using TIs and heavy metals (Table I). Besides the effective spin Hall angle θ_{SH} and the critical current for switching J_{cr}, we list the power consumption for switching ferromagnetic electrodes in unit magnetic volume, expressed as J_{cr}^2/σ, where σ is the electrical conductivity of the spin–orbit materials. We can see that TIs stand out as the favorable materials for magnetic switching because they benefit from reduced critical current and low power consumption. However, J_{cr} not only depends on the properties of the TI layer but is also affected by the thermal stability of the ferromagnetic layer as well as the applied in-plane bias field in experiments with PMA materials. To reveal the intrinsic SOT generation, one can replace J_{cr} by $1/\theta_{SH}$ because in spin–orbit materials with the same geometrical dimensions, the critical current density for switching scales with the inverse of the spin Hall angle. We find that TIs still represent an energy efficient candidate when $1/\theta_{SH}^2\sigma$, or equivalently σ/σ_{SH}^2, is adopted as the comparison metric (σ_{SH} is the spin Hall conductivity). These features suggest that the strategy of utilizing conductive surface states with strong spin-momentum locking is desired for maximizing the SOT and power efficiency. In reality, it may not be very rigorous to directly compare the absolute values of SOT efficiencies from different works because the actual values depend heavily on the details of the sample quality and experimental technique in each study. Nevertheless, some presentations of SOT and power efficiencies may still be useful to capture the main features. For a fairer comparison, it is helpful to measure on different materials using the same technique within one particular study.[41,63,68]

We would like to emphasize here that in the majority of existing TI/ferromagnet devices, a large portion of the applied current flows in the conductive ferromagnetic layer, which has not been taken into account in the power calculation above. Considering the "wasted" power in ferromagnetic metals, the comparison on power consumption in Table I can look differently, where some of the recently studied heavy metal alloys exhibit very competitive power performances.[80,81] The unnecessary dissipation from magnetic metals can be potentially avoided by using an insulator as the magnetic free layer, developing more conductive TIs, or inserting an insulator between the TI and the ferromagnet, which has been discussed above.

We note that in Table I, the spin Hall angle of many TI films is larger than unity. In the original definition of the three-dimensional spin Hall effect in the diffusive region, $\theta_{SH} = (2e/\hbar)J_s/J_c$ represents the ratio between the transverse spin current density and longitudinal charge current density. Therefore, θ_{SH} should be interpreted as the tangent of the angle formed by the electrons' trajectory and the longitudinal direction. In the case of a small deflection angle, the

© Author(s) 2021

TABLE I. Summary of the key parameters in the SOT switching experiments using TIs and heavy metals.

Parameters	Reference 31	Reference 39	Reference 41	Reference 71	Reference 70	Reference 30	Reference 68	Reference 78	Reference 3
Spin–orbit material	$(Bi,Sb)_2Te_3$	$(Bi,Sb)_2Te_3$	Bi_2Se_3	Bi_2Se_3	$Bi_{0.9}Sb_{0.1}$	Bi_xSe_{1-x}	$(Bi,Sb)_2Te_3$	Bi_2Se_3	Pt
Ferromagnet	Cr-$(Bi,Sb)_2Te_3$	Cr-$(Bi,Sb)_2Te_3$	CoTb	NiFe[a]	MnGa	CoFeB[b]	GdFeCo	$BaFe_{12}O_{19}$	Co
Substrate	GaAs (111)	InP (111)	GaAs (111)	Al_2O_3 (0001)	GaAs (001)	SiO_2	Al_2O_3 (0001)	Al_2O_3 (0001)	SiO_2
Temperature (K)	1.9	2	RT[c]	RT	RT	RT	RT	3–200	RT
Spin Hall angle θ_{SH}	140	...[c]	0.16	1	52	18.6	3	267 (3 K)	0.03
Conductivity σ (S/cm)	220	...	943	400	2.5×10^3	78	182	660–760	2×10^4
Critical current J_{cr} (A/cm^2)	8.9×10^4	2.5×10^6	2.8×10^6	6×10^5	1.5×10^6	4.3×10^5	1.2×10^5	$1–2 \times 10^6$	2.8×10^7
Power ${J_{cr}}^2/\sigma$ (W/cm^3)	3.6×10^7	...	8.3×10^9	9×10^8	9×10^8	1.3×10^9	7.9×10^9	$2–6 \times 10^9$	1.4×10^{10}
$1/({\theta_{SH}}^2\sigma)$ normalized with Pt	4×10^{-6}	...	0.7	0.05	3×10^{-6}	7×10^{-4}	0.01	3×10^{-7}	1

[a]NiFe has in-plane magnetic anisotropy. Other ferromagnets in this table have PMA.
[b]CoFeB here represents a multilayer containing Ta/CoFeB/Gd/CoFeB.
[c]"..." means information not shown in the reference. RT means room temperature.

so-defined spin Hall angle is close to the angle of the trajectory. In the extreme case that the trajectory angle gets close to 90°, the spin Hall angle goes toward infinity. In this sense, the larger-than-unity spin Hall angle is a natural reflection of the "quantum spin Hall state" that is expected from high quality topological insulators.

IV. CONCLUSIONS AND OUTLOOK

Thanks to the tremendous efforts from the TI and the spintronic communities in developing high quality TI films and characterizing the outstanding SOT efficiency, TIs have been recognized as a promising candidate for building magnetic memory devices with ultralow dissipation. However, there are still a few bottlenecks to be overcome before TIs can be readily used as the spin current source in real applications. In most of the existing studies, the synthesis of TI films requires the costly technique of molecular beam epitaxy. Deposition techniques that are more compatible with the CMOS manufacture process should be developed to produce TI films with large scale. As discussed earlier, the sputtered Bi_xSe_{1-x} film provides an industry-friendly approach that explores the giant SOT.[30] Furthermore, for practical magnetic random-access memory technology, TIs need to be integrated with the state-of-the-art magnetic tunnel junctions, for example, CoFeB/MgO/CoFeB stacks with PMA and tunneling magnetoresistance (TMR) bigger than 100%.[82] Engineering the TI surface that can support the PMA of magnetic layers and avoid atomic diffusion during high-temperature fabrication would be a critical step. Possible ways include developing TI films or adding insertion layers with good thermal stability and appropriate crystal orientation, which helps in forming (001)-oriented CoFeB.[83] As a final goal, a demonstration of magnetic tunnel junctions integrated with TI layers that have high TMR and efficient SOT switching are highly desirable for the practical applications of TI-based spintronics.[84]

Besides the potential improvements in practical devices, there remain many open questions on the fundamental interpretation of the TI induced SOT phenomena, even on the basic effect in the simplest sample structure, i.e., the switching and efficiency in the TI/ferromagnet bilayer. First of all, it is not fully understood why the experimentally determined charge-spin conversion efficiency varies significantly among different TI systems. Besides variances in the sample quality and measurement technique, there exists a more fundamental question on how to determine the contributions from the bulk and surface. As is discussed earlier in this review, besides the intrinsic topological bulk bands that give rise to the surface states, it seems that in experiments the bulk states can make additional contributions through extrinsic non-topological effects. How to separate the topological trivial and non-trivial effects in SOT remains a challenging task. Moreover, regarding the topological non-trivial origin, it will be helpful to correlate the SOT with the structure of surface bands in the same material stack. As a good starting point, people have combined spin pumping with ARPES in a TI material α-Sn, where the spin-to-charge conversion coexists with the topological surface states.[25]

There exist many other interesting topics beyond the traditional scheme of switching ferromagnetic materials. So far, TIs have mostly been used to generate in-plane spins to switch PMA materials, which provides better thermal stability than in-plane magnets.[82] Since the

© Author(s) 2021

spins are perpendicular to the easy axis of the magnet, the damping-like SOT plays the role as an effective magnetic field, which needs to overcome the anisotropy field in the order of 0.1–1 T for reaching magnetic switching in a thermally stable nanomagnet, thus requiring a huge current density. However, when the spins are collinear with the magnetic easy axis, the switching current can be largely reduced because the SOT is used to overcome the Gilbert damping.[4,85] Therefore, it is highly desired to switch PMA materials with out-of-plane spins.[86–90] Designing TI structures with low symmetry along the certain crystal direction is a promising way to generate out-of-plane spins[87,91] while benefiting from the demonstrated giant charge-to-spin conversion. Finally, we highlight the rich physics and applications when combining TIs with antiferromagnets. On one hand, the antiferromagnetic exchange coupling[92–94] with the Dirac fermions at the interface can give rise to emergent phenomena such as topologically nontrivial spin textures.[95] On the other hand, the giant SOT from TIs can be potentially used to displace the spin texture and switch the Néel vector. In addition, the recently demonstrated picosecond-timescale charge-spin conversion in TIs[96] has great potential to be accompanied with the ultrafast dynamics of antiferromagnets. In a word, we believe that many opportunities in both fundamental investigation and application of topological spintronics have emerged on the horizon.

ACKNOWLEDGMENTS

The authors acknowledge the support from the National Science Foundation under Grant No. ECCS-1653553 and the Semiconductor Research Corporation.

DATA AVAILABILITY

Data sharing is not applicable to this article as no new data were created or analyzed in this study.

REFERENCES

[1] A. Manchon, J. Železný, I. M. Miron, T. Jungwirth, J. Sinova, A. Thiaville, K. Garello, and P. Gambardella, Rev. Mod. Phys. **91**, 035004 (2019).
[2] I. M. Miron, K. Garello, G. Gaudin, P.-J. Zermatten, M. V. Costache, S. Auffret, S. Bandiera, B. Rodmacq, A. Schuhl, and P. Gambardella, Nature **476**, 189 (2011).
[3] L. Liu, O. J. Lee, T. J. Gudmundsen, D. C. Ralph, and R. A. Buhrman, Phys. Rev. Lett. **109**, 096602 (2012).
[4] L. Liu, C.-F. Pai, Y. Li, H. W. Tseng, D. C. Ralph, and R. A. Buhrman, Science **336**, 555 (2012).
[5] C.-F. Pai, L. Liu, Y. Li, H. W. Tseng, D. C. Ralph, and R. A. Buhrman, Appl. Phys. Lett. **101**, 122404 (2012).
[6] A. Hoffmann, IEEE Trans. Magn. **49**, 5172 (2013).
[7] A. Manchon, H. C. Koo, J. Nitta, S. M. Frolov, and R. A. Duine, Nat. Mater. **14**, 871 (2015).
[8] A. Soumyanarayanan, N. Reyren, A. Fert, and C. Panagopoulos, Nature **539**, 509 (2016).
[9] P. M. Haney, H. W. Lee, K. J. Lee, A. Manchon, and M. D. Stiles, Phys. Rev. B **87**, 174411 (2013).
[10] R. Ramaswamy, J. M. Lee, K. Cai, and H. Yang, Appl. Phys. Rev. **5**, 031107 (2018).
[11] L. Fu, C. L. Kane, and E. J. Mele, Phys. Rev. Lett. **98**, 106803 (2007).
[12] H. Zhang, C.-X. Liu, X.-L. Qi, X. Dai, Z. Fang, and S.-C. Zhang, Nat. Phys. **5**, 438 (2009).
[13] Y. L. Chen, J. G. Analytis, J.-H. Chu, Z. K. Liu, S.-K. Mo, X. L. Qi, H. J. Zhang, D. H. Lu, X. Dai, Z. Fang, S. C. Zhang, I. R. Fisher, Z. Hussain, and Z.-X. Shen, Science **325**, 178 (2009).
[14] D. Hsieh, Y. Xia, D. Qian, L. Wray, J. H. Dil, F. Meier, J. Osterwalder, L. Patthey, J. G. Checkelsky, N. P. Ong, A. V. Fedorov, H. Lin, A. Bansil, D. Grauer, Y. S. Hor, R. J. Cava, and M. Z. Hasan, Nature **460**, 1101 (2009).
[15] M. Z. Hasan and C. L. Kane, Rev. Mod. Phys. **82**, 3045 (2010).
[16] X.-L. Qi and S.-C. Zhang, Rev. Mod. Phys. **83**, 1057 (2011).
[17] H. Wang, J. Kally, C. Şahin, T. Liu, W. Yanez, E. J. Kamp, A. Richardella, M. Wu, M. E. Flatté, and N. Samarth, Phys. Rev. Res. **1**, 012014(R) (2019).
[18] Z. Chi, Y.-C. Lau, X. Xu, T. Ohkubo, K. Hono, and M. Hayashi, Sci. Adv. **6**, eaay2324 (2020).
[19] P. Deorani, J. Son, K. Banerjee, N. Koirala, M. Brahlek, S. Oh, and H. Yang, Phys. Rev. B **90**, 094403 (2014).
[20] M. Jamali, J. S. Lee, J. S. Jeong, F. Mahfouzi, Y. Lv, Z. Zhao, B. K. Nikolić, K. A. Mkhoyan, N. Samarth, and J.-P. Wang, Nano Lett. **15**, 7126 (2015).
[21] Y. Zhang, K. He, C.-Z. Chang, C.-L. Song, L.-L. Wang, X. Chen, J.-F. Jia, Z. Fang, X. Dai, W.-Y. Shan, S.-Q. Shen, Q. Niu, X.-L. Qi, S.-C. Zhang, X.-C. Ma, and Q.-K. Xue, Nat. Phys. **6**, 584 (2010).
[22] C.-Z. Chang, J. Zhang, X. Feng, J. Shen, Z. Zhang, M. Guo, K. Li, Y. Ou, P. Wei, L.-L. Wang, Z.-Q. Ji, Y. Feng, S. Ji, X. Chen, J. Jia, X. Dai, Z. Fang, S.-C. Zhang, K. He, Y. Wang, L. Lu, X.-C. Ma, and Q.-K. Xue, Science **340**, 167 (2013).
[23] A. Richardella, D. M. Zhang, J. S. Lee, A. Koser, D. W. Rench, A. L. Yeats, B. B. Buckley, D. D. Awschalom, and N. Samarth, Appl. Phys. Lett. **97**, 262104 (2010).
[24] J. Zhang, C.-Z. Chang, Z. Zhang, J. Wen, X. Feng, K. Li, M. Liu, K. He, L. Wang, X. Chen, Q.-K. Xue, X. Ma, and Y. Wang, Nat. Commun. **2**, 574 (2011).
[25] J.-C. Rojas-Sánchez, S. Oyarzún, Y. Fu, A. Marty, C. Vergnaud, S. Gambarelli, L. Vila, M. Jamet, Y. Ohtsubo, A. Taleb-Ibrahimi, P. Le Fèvre, F. Bertran, N. Reyren, J.-M. George, and A. Fert, Phys. Rev. Lett. **116**, 096602 (2016).
[26] Q. Song, J. Mi, D. Zhao, T. Su, W. Yuan, W. Xing, Y. Chen, T. Wang, T. Wu, X. H. Chen, X. C. Xie, C. Zhang, J. Shi, and W. Han, Nat. Commun. **7**, 13485 (2016).
[27] T. Liu, Y. Li, L. Gu, J. Ding, H. Chang, P. A. P. Janantha, B. Kalinikos, V. Novosad, A. Hoffmann, R. Wu, C. L. Chien, and M. Wu, Phys. Rev. Lett. **120**, 207206 (2018).
[28] Y. Li, Q. Ma, S. X. Huang, and C. L. Chien, Sci. Adv. **4**, eaap8294 (2018).
[29] J. Kim, C. Jang, X. Wang, J. Paglione, S. Hong, S. Sayed, D. Chun, and D. Kim, Phys. Rev. B **102**, 054410 (2020).
[30] M. Dc, R. Grassi, J.-Y. Chen, M. Jamali, D. R. Hickey, D. Zhang, Z. Zhao, H. Li, P. Quarterman, Y. Lv, M. Li, A. Manchon, K. A. Mkhoyan, T. Low, and J.-P. Wang, Nat. Mater. **17**, 800 (2018).
[31] Y. Fan, P. Upadhyaya, X. Kou, M. Lang, S. Takei, Z. Wang, J. Tang, L. He, L.-T. Chang, M. Montazeri, G. Yu, W. Jiang, T. Nie, R. N. Schwartz, Y. Tserkovnyak, and K. L. Wang, Nat. Mater. **13**, 699 (2014).
[32] A. R. Mellnik, J. S. Lee, A. Richardella, J. L. Grab, P. J. Mintun, M. H. Fischer, A. Vaezi, A. Manchon, E.-A. Kim, N. Samarth, and D. C. Ralph, Nature **511**, 449 (2014).
[33] U. H. Pi, K. W. Kim, J. Y. Bae, S. C. Lee, Y. J. Cho, K. S. Kim, and S. Seo, Appl. Phys. Lett. **97**, 162507 (2010).
[34] J. Kim, J. Sinha, M. Hayashi, M. Yamanouchi, S. Fukami, T. Suzuki, S. Mitani, and H. Ohno, Nat. Mater. **12**, 240 (2013).
[35] X. Che, Q. Pan, B. Vareskic, J. Zou, L. Pan, P. Zhang, G. Yin, H. Wu, Q. Shao, P. Deng, and K. L. Wang, Adv. Mater. **32**, 1907661 (2020).
[36] L. Liu, T. Moriyama, D. C. Ralph, and R. A. Buhrman, Phys. Rev. Lett. **106**, 036601 (2011).
[37] Y. Wang, P. Deorani, K. Banerjee, N. Koirala, M. Brahlek, S. Oh, and H. Yang, Phys. Rev. Lett. **114**, 257202 (2015).
[38] C.-F. Pai, M. Mann, A. J. Tan, and G. S. D. Beach, Phys. Rev. B **93**, 144409 (2016).
[39] K. Yasuda, A. Tsukazaki, R. Yoshimi, K. Kondou, K. S. Takahashi, Y. Otani, M. Kawasaki, and Y. Tokura, Phys. Rev. Lett. **119**, 137204 (2017).
[40] N. Roschewsky, E. S. Walker, P. Gowtham, S. Muschinske, F. Hellman, S. R. Bank, and S. Salahuddin, Phys. Rev. B **99**, 195103 (2019).
[41] J. Han, A. Richardella, S. A. Siddiqui, J. Finley, N. Samarth, and L. Liu, Phys. Rev. Lett. **119**, 077702 (2017).

© Author(s) 2021

[42]Y. Shiomi, K. Nomura, Y. Kajiwara, K. Eto, M. Novak, K. Segawa, Y. Ando, and E. Saitoh, Phys. Rev. Lett. **113**, 196601 (2014).
[43]A. A. Baker, A. I. Figueroa, L. J. Collins-Mcintyre, G. van der Laan, and T. Hesjedal, Sci. Rep. **5**, 7907 (2015).
[44]A. Azevedo, L. H. Vilela-Leão, R. L. Rodríguez-Suárez, A. F. Lacerda Santos, and S. M. Rezende, Phys. Rev. B **83**, 144402 (2011).
[45]S. Y. Huang, W. G. Wang, S. F. Lee, J. Kwo, and C. L. Chien, Phys. Rev. Lett. **107**, 216604 (2011).
[46]L. Bai, P. Hyde, Y. S. Gui, C.-M. Hu, V. Vlaminck, J. E. Pearson, S. D. Bader, and A. Hoffmann, Phys. Rev. Lett. **111**, 217602 (2013).
[47]Y. T. Fanchiang, K. H. M. Chen, C. C. Tseng, C. C. Chen, C. K. Cheng, S. R. Yang, C. N. Wu, S. F. Lee, M. Hong, and J. Kwo, Nat. Commun. **9**, 223 (2018).
[48]A. Nomura, N. Nasaka, T. Tashiro, T. Sasagawa, and K. Ando, Phys. Rev. B **96**, 214440 (2017).
[49]C. Tang, Q. Song, C.-Z. Chang, Y. Xu, Y. Ohnuma, M. Matsuo, Y. Liu, W. Yuan, Y. Yao, J. S. Moodera, S. Maekawa, W. Han, and J. Shi, Sci. Adv. **4**, eaas8660 (2018).
[50]S. Gupta, S. Kanai, F. Matsukura, and H. Ohno, AIP Adv. **7**, 055919 (2017).
[51]Z. Jiang, C.-Z. Chang, M. R. Masir, C. Tang, Y. Xu, J. S. Moodera, A. H. MacDonald, and J. Shi, Nat. Commun. **7**, 11458 (2016).
[52]C. H. Li, O. M. J. van't Erve, J. T. Robinson, Y. Liu, L. Li, and B. T. Jonker, Nat. Nanotechnol. **9**, 218 (2014).
[53]Y. Ando, T. Hamasaki, T. Kurokawa, K. Ichiba, F. Yang, M. Novak, S. Sasaki, K. Segawa, Y. Ando, and M. Shiraishi, Nano Lett. **14**, 6226 (2014).
[54]J. Tang, L.-T. Chang, X. Kou, K. Murata, E. S. Choi, M. Lang, Y. Fan, Y. Jiang, M. Montazeri, W. Jiang, Y. Wang, L. He, and K. L. Wang, Nano Lett. **14**, 5423 (2014).
[55]A. Dankert, J. Geurs, M. V. Kamalakar, S. Charpentier, and S. P. Dash, Nano Lett. **15**, 7976 (2015).
[56]F. Yang, S. Ghatak, A. A. Taskin, K. Segawa, Y. Ando, M. Shiraishi, Y. Kanai, K. Matsumoto, A. Rosch, and Y. Ando, Phys. Rev. B **94**, 075304 (2016).
[57]J. Tian, I. Miotkowski, S. Hong, and Y. P. Chen, Sci. Rep. **5**, 14293 (2015).
[58]K. Vaklinova, A. Hoyer, M. Burghard, and K. Kern, Nano Lett. **16**, 2595 (2016).
[59]E. K. de Vries, A. M. Kamerbeek, N. Koirala, M. Brahlek, M. Salehi, S. Oh, B. J. van Wees, and T. Banerjee, Phys. Rev. B **92**, 201102(R) (2015).
[60]L. Liu, A. Richardella, I. Garate, Y. Zhu, N. Samarth, and C.-T. Chen, Phys. Rev. B **91**, 235437 (2015).
[61]P. He, S. S.-L. Zhang, D. Zhu, Y. Liu, Y. Wang, J. Yu, G. Vignale, and H. Yang, Nat. Phys. **14**, 495 (2018).
[62]K. Kondou, R. Yoshimi, A. Tsukazaki, Y. Fukuma, J. Matsuno, K. S. Takahashi, M. Kawasaki, Y. Tokura, and Y. Otani, Nat. Phys. **12**, 1027 (2016).
[63]H. Wu, P. Zhang, P. Deng, Q. Lan, Q. Pan, S. A. Razavi, X. Che, L. Huang, B. Dai, K. Wong, X. Han, and K. L. Wang, Phys. Rev. Lett. **123**, 207205 (2019).
[64]Y. Fan, X. Kou, P. Upadhyaya, Q. Shao, L. Pan, M. Lang, X. Che, J. Tang, M. Montazeri, K. Murata, L.-T. Chang, M. Akyol, G. Yu, T. Nie, K. L. Wong, J. Liu, Y. Wang, Y. Tserkovnyak, and K. L. Wang, Nat. Nanotechnol. **11**, 352 (2016).
[65]H. Wang, J. Kally, J. S. Lee, T. Liu, H. Chang, D. R. Hickey, K. A. Mkhoyan, M. Wu, A. Richardella, and N. Samarth, Phys. Rev. Lett. **117**, 076601 (2016).
[66]P. Hansen, S. Klahn, C. Clausen, G. Much, and K. Witter, J. Appl. Phys. **69**, 3194 (1991).
[67]J. Finley and L. Liu, Phys. Rev. Appl. **6**, 054001 (2016).
[68]H. Wu, Y. Xu, P. Deng, Q. Pan, S. A. Razavi, K. Wong, L. Huang, B. Dai, Q. Shao, G. Yu, X. Han, J. C. Rojas-Sánchez, S. Mangin, and K. L. Wang, Adv. Mater. **31**, 1901681 (2019).
[69]Q. Shao, H. Wu, Q. Pan, P. Zhang, L. Pan, K. Wong, X. Che, and K. L. Wang, in *2018 IEEE International Electron Devices Meeting (IEDM), San Francisco, CA* (IEEE, 2018), p. 36.3.1.
[70]N. H. D. Khang, Y. Ueda, and P. N. Hai, Nat. Mater. **17**, 808 (2018).
[71]Y. Wang, D. Zhu, Y. Wu, Y. Yang, J. Yu, R. Ramaswamy, R. Mishra, S. Shi, M. Elyasi, K.-L. Teo, Y. Wu, and H. Yang, Nat. Commun. **8**, 1364 (2017).
[72]K. Yasuda, A. Tsukazaki, R. Yoshimi, K. S. Takahashi, M. Kawasaki, and Y. Tokura, Phys. Rev. Lett. **117**, 127202 (2016).
[73]Y. Lv, J. Kally, D. Zhang, J. S. Lee, M. Jamali, N. Samarth, and J.-P. Wang, Nat. Commun. **9**, 111 (2018).
[74]Y. Fan, Q. Shao, L. Pan, X. Che, Q. He, G. Yin, C. Zheng, G. Yu, T. Nie, M. R. Masir, A. H. MacDonald, and K. L. Wang, Nano Lett. **19**, 692 (2019).
[75]M. Dc, J.-Y. Chen, T. Peterson, P. Sahu, B. Ma, N. Mousavi, R. Harjani, and J.-P. Wang, Nano Lett. **19**, 4836 (2019).
[76]Z. Zheng, D. Zhu, K. Zhang, X. Feng, Y. He, L. Chen, Z. Zhang, D. Liu, Y. Zhang, P. K. Amiri, and W. Zhao, Chin. Phys. B **29**, 078505 (2020).
[77]C. O. Avci, A. Quindeau, C.-F. Pai, M. Mann, L. Caretta, A. S. Tang, M. C. Onbasli, C. A. Ross, and G. S. D. Beach, Nat. Mater. **16**, 309 (2017).
[78]P. Li, J. Kally, S. S.-L. Zhang, T. Pillsbury, J. Ding, G. Csaba, J. Ding, J. S. Jiang, Y. Liu, R. Sinclair, C. Bi, A. DeMann, G. Rimal, W. Zhang, S. B. Field, J. Tang, W. Wang, O. G. Heinonen, V. Novosad, A. Hoffmann, N. Samarth, and M. Wu, Sci. Adv. **5**, eaaw3415 (2019).
[79]Y. Wang, D. Zhu, Y. Yang, K. Lee, R. Mishra, G. Go, S.-H. Oh, D.-H. Kim, K. Cai, E. Liu, S. D. Pollard, S. Shi, J. Lee, K. L. Teo, Y. Wu, K.-J. Lee, and H. Yang, Science **366**, 1125 (2019).
[80]L. Zhu, D. C. Ralph, and R. A. Buhrman, Phys. Rev. Appl. **10**, 031001 (2018).
[81]X. Li, S.-J. Lin, M. Dc, Y.-C. Liao, C. Yao, A. Naeemi, W. Tsai, and S. X. Wang, in *2019 IEEE SOI-3D-Subthreshold Microelectronics Technology Unified Conference (S3S), San Jose, CA* (IEEE, 2019).
[82]S. Ikeda, K. Miura, H. Yamamoto, K. Mizunuma, H. D. Gan, M. Endo, S. Kanai, J. Hayakawa, F. Matsukura, and H. Ohno, Nat. Mater. **9**, 721 (2010).
[83]D. C. Worledge, G. Hu, D. W. Abraham, P. L. Trouilloud, and S. Brown, J. Appl. Phys. **115**, 172601 (2014).
[84]C.-F. Pai, Nat. Mater. **17**, 755 (2018).
[85]S. Fukami, T. Anekawa, C. Zhang, and H. Ohno, Nat. Nanotechnol. **11**, 621 (2016).
[86]S.-H. C. Baek, V. P. Amin, Y.-W. Oh, G. Go, S.-J. Lee, G.-H. Lee, K.-J. Kim, M. D. Stiles, B.-G. Park, and K.-J. Lee, Nat. Mater. **17**, 509 (2018).
[87]L. Liu, C. Zhou, X. Shu, C. Li, T. Zhao, W. Lin, J. Deng, Q. Xie, S. Chen, J. Zhou, R. Guo, H. Wang, J. Yu, S. Shi, P. Yang, S. Pennycook, A. Manchon, and J. Chen, Nat. Nanotechnol. **16**, 277 (2021).
[88]X. Chen, S. Shi, G. Shi, X. Fan, C. Song, X. Zhou, H. Bai, L. Liao, Y. Zhou, H. Zhang, A. Li, Y. Chen, X. Han, S. Jiang, Z. Zhu, H. Wu, X. Wang, D. Xue, H. Yang, and F. Pan, Nat. Mater. (published online 2021).
[89]M. Dc, D.-F. Shao, V. D.-H. Hou, P. Quarterman, A. Habiboglu, B. Venuti, M. Miura, B. Kirby, A. Vailionis, C. Bi, X. Li, F. Xue, Y.-L. Huang, Y. Deng, S.-J. Lin, W. Tsai, S. Eley, W. Wang, J. A. Borchers, E. Y. Tsymbal, and S. X. Wang, arXiv:2012.09315 (2020).
[90]S. Hu, D.-F. Shao, H. Yang, M. Tang, Y. Yang, W. Fan, S. Zhou, E. Y. Tsymbal, and X. Qiu, arXiv:2103.09011 (2021).
[91]D. MacNeill, G. M. Stiehl, M. H. D. Guimaraes, R. A. Buhrman, J. Park, and D. C. Ralph, Nat. Phys. **13**, 300 (2017).
[92]Q. L. He, X. Kou, A. J. Grutter, G. Yin, L. Pan, X. Che, Y. Liu, T. Nie, B. Zhang, S. M. Disseler, B. J. Kirby, W. Ratcliff II, Q. Shao, K. Murata, X. Zhu, G. Yu, Y. Fan, M. Montazeri, X. Han, J. A. Borchers, and K. L. Wang, Nat. Mater. **16**, 94 (2017).
[93]F. Wang, D. Xiao, W. Yuan, J. Jiang, Y.-F. Zhao, L. Zhang, Y. Yao, W. Liu, Z. Zhang, C. Liu, J. Shi, W. Han, M. H. W. Chan, N. Samarth, and C.-Z. Chang, Nano Lett. **19**, 2945 (2019).
[94]C.-Y. Yang, L. Pan, A. J. Grutter, H. Wang, X. Che, Q. L. He, Y. Wu, D. A. Gilbert, P. Shafer, E. Arenholz, H. Wu, G. Yin, P. Deng, J. A. Borchers, W. Ratcliff II, and K. L. Wang, Sci. Adv. **6**, eaaz8463 (2020).
[95]Q. L. He, G. Yin, A. J. Grutter, L. Pan, X. Che, G. Yu, D. A. Gilbert, S. M. Disseler, Y. Liu, P. Shafer, B. Zhang, Y. Wu, B. J. Kirby, E. Arenholz, R. K. Lake, X. Han, and K. L. Wang, Nat. Commun. **9**, 2767 (2018).
[96]X. Wang, L. Cheng, D. Zhu, Y. Wu, M. Chen, Y. Wang, D. Zhao, C. B. Boothroyd, Y. M. Lam, J. X. Zhu, M. Battiato, J. C. W. Song, H. Yang, and E. E. M. Chia, Adv. Mater. **30**, 1802356 (2018).

© Author(s) 2021